Multivariable-PI-Based *dq* Current Control of Voltage Source Converters With Superior Axis Decoupling Capability

Behrooz Bahrani, *Student Member, IEEE*, Stephan Kenzelmann, *Student Member, IEEE*, and Alfred Rufer, *Fellow, IEEE*

***Abstract*—This paper presents a linear direct–quadrature current control strategy for voltage source converters (VSCs) in a rotating reference frame (RRF). The described method is based on multivariable-proportional–integral (PI) regulators and provides fast dynamics and a zero steady-state error. Contrary to the well-known conventional PI-based control strategies in RRFs, the presented method provides practically decoupled axes with a superior disturbance rejection capability. Moreover, its implementation is relatively simple and does not impose excessive structural complexity compared to its conventional PI-based competitors. The method is applicable to both single- and three-phase systems and also to anisotropic three-phase systems, e.g., synchronous motors with different direct and quadrature impedances driven by VSCs. Implementing a three-phase test system, the performance of the presented method is experimentally evaluated.**

***Index Terms*—Current control, multivariable-proportional–integral (PI) controllers, stationary and rotating reference frames, vector control, voltage source converters (VSCs).**

I. Introduction

POWER inverters with regulated input currents are widely utilized in many grid-tied applications, e.g., distributed power generation with renewable energy resources such as photovoltaic energy [2], [3] and wind energy [4], HVdc applications [5], active power filters [6]–[8], power factor controllers [9], [10], etc. Recently, the high depth of penetration of distributed energy resources has also intensified the demand for such inverters. In most of such applications, a voltage source converter (VSC) is interfaced to the utility grid through a line reactor filter, and a current regulation scheme is adopted by the VSC to control its input current while the dc link voltage is regulated by a relatively slower control loop compared to that of the current [11].

Over the years, considerable research has been conducted on the current regulation of VSCs, and various approaches have been proposed [12]–[23]. Generally, these approaches can be categorized into two major classes: 1) linear and 2) nonlinear controllers [12]. Nonlinear approaches [13], [14] normally impose structural complexity but do not offer impressive and superior performance compared to that of linear schemes. However, the structural simplicity and fully digital implementability of linear control strategies, specifically stationary reference frame (SRF)- and rotating reference frame (RRF)-based controllers, have made them so popular. Among the SRF controllers, the simple and linear proportional–integral (PI) controllers are considered as the most conventional approach. However, due to their well-known drawbacks, e.g., a nonzero steady-state error, other approaches such as SRF-based proportional–resonant (PR) [16]–[18] controllers have been proposed, which track ac references in the stationary frame with a zero steady-state error. The PR approach is based on providing an infinite gain at the target frequency for eliminating the steady-state error at that frequency, which is virtually similar to the infinite gain of a PI controller at dc. Although the PR approach is relatively simple and easy to implement for both single- and three-phase applications, however, it suffers from several drawbacks, e.g., sensitivity to grid frequency variations, exponentially decaying transients during step changes, and being pushed toward instability margins even by a small phase shift introduced by the adopted current sensors [16].

Among the RRF controllers, the PI regulators are the most well-known and easy-to-implement approaches which provide a satisfactory performance, i.e., fast dynamics and a zero steady-state error. The PI-based current regulation approach is originally proposed in [15] and is extensively studied and adopted for the current control of both single- and three-phase systems in various applications [2], [3], [5], [9]–[12], [15], [24]–[32]. In an RRF, usually referred to as a dq frame, ac (time varying) quantities appear as direct and quadrature (d and q) dc (time invariant) quantities allowing the controller to be designed as dc–dc converters presenting an infinite control gain at the steady-state operating point for a zero steady-state error. In the proposed control strategy of [15], two distinct current axes, i.e., d and q axes, are identified, which are aimed to be independently regulated. However, due to the structure of the PI-based controller, the d and q axes are not fully decoupled, and each axis acts as a disturbance for the other one. Since PI controllers inherently have poor disturbance rejection capabilities, step changes in one axis generate transients in the other one, which might last even several cycles and leads to power quality and performance degradation.

Manuscript received November 19, 2009; revised April 23, 2010 and July 16, 2010; accepted July 31, 2010. Date of publication August 30, 2010; date of current version June 15, 2011.

The authors are with the Laboratoire dÉlectronique Industrielle, Ecole Polytechnique Fédérale de Lausanne, 1015 Lausanne, Switzerland (e-mail: behrooz.bahrani@a3.epfl.ch; stephan.kenzelmann@a3.epfl.ch; alfred.rufer@epfl.ch).

Color versions of one or more of the figures in this paper are available online at http://ieeexplore.ieee.org.

Digital Object Identifier 10.1109/TIE.2010.2070776

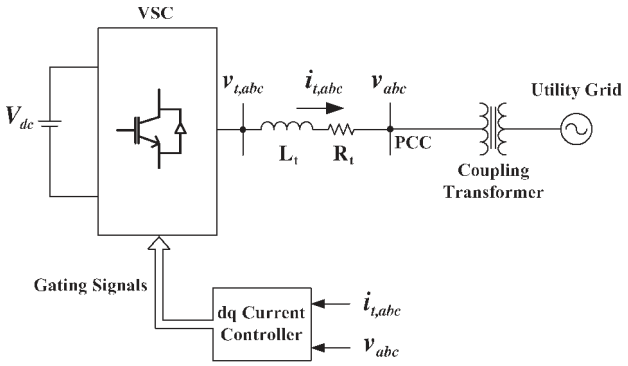

Fig. 1. One-line diagram of the three-phase test system.

The extensive range of applications of PI-based current regulation strategies provides strong incentives to explore alternative current regulation schemes with similar structural simplicity and dynamics responses that can overcome the aforementioned shortcoming. This paper presents a PI-based current regulation scheme for VSCs, i.e., a multivariable-PI controller, in which the d and q axes are almost fully decoupled such that the step changes in one axis negligibly affect the other one [1]. Similar to the conventional PI-based approaches, the presented method has the following characteristics: 1) provides a satisfactory performance, e.g., fast dynamics and a zero steady-state error, and 2) is structurally simple. In this paper, the system modeling and design procedure corresponding to the multivariable-PI control strategy are presented, and its performance is experimentally evaluated for three-phase systems. Moreover, its performance is compared to that of the conventional current regulation approach. Note that the purposes of the presented paper are as follows: 1) implementing the control strategy proposed by Prof. H. Bühler in [1] in real time; 2) comparing it with another well-known strategy; and 3) diffusing the knowledge within the English speaking community.

The rest of this paper is organized as follows. Section II describes the utilized test systems and provides a mathematical model for the adopted three-phase system. Section III briefly reviews the conventional PI-based current regulation scheme. Section IV describes the multivariable-PI current control strategy. Section V experimentally evaluates the performance of the method and compares it with that of the conventional approach, and Section VI concludes this paper.

II. System Description and Modeling

To evaluate the performance of the multivariable-PI control strategy, a three-phase test system is adopted. Fig. 1 shows a one-line schematic diagram of the adopted test system in which a VSC-based power conversion system is connected to the utility grid through a series line reactor filter and a coupling transformer. The filter is represented by inductance L_t and its associated internal resistance R_t for each phase. The inductance also accounts for the leakage inductance of the interface transformer between the grid and the filter. The parameters of the adopted three-phase test system are given in Table I.

TABLE I
Parameters of the Three-Phase Test System

Quantity	Value	Comment
L_t	5 *mH* (0.125 pu)	Inductance of VSC Filter
R_t	0.15 Ω (0.012 pu)	Resistance of VSC Filter
VSC rated power	0.8 kW (1 pu)	S_{base} = 0.8 kVA
V_{dc}	300 V	DC Bus Voltage
V_s	230 V (rms) (1 pu)	Ph-G Grid Nominal Voltage
$n_1 : n_2$	4:1	Transformer Ratio
f_{sw}	10 kHz	PWM Carrier Frequency
f_s	5 kHz	Sampling Frequency
f	50 Hz	System Nominal Frequency
ω	314.15 rad/s	Nominal Angular Frequency

A. Mathematical Model

In this section, the mathematical model of the three-phase system in Fig. 1 is described, and a structural diagram of that is derived, which is adopted for the design of the controllers in the following sections.

Based on the system in Fig. 1, the dynamics of the VSC ac-side variables can be described in an abc frame as follows:

$$v_{t,\mathrm{abc}} = R_t i_{t,\mathrm{abc}} + L_t \frac{di_{t,\mathrm{abc}}}{dt} + v_{\mathrm{abc}} \tag{1}$$

in which $v_{t,\mathrm{abc}}$ and v_{abc} are the VSC terminal voltages and the grid voltages, respectively, L_t and R_t are the parameters of the line reactor filter, and $i_{t,\mathrm{abc}}$ is the line current. Transforming (1) from the abc frame to a stationary $\alpha\beta 0$ frame, the following equation is obtained:

$$v_{t,\alpha\beta 0} = R_t i_{t,\alpha\beta 0} + L_t \frac{di_{t,\alpha\beta 0}}{dt} + v_{\alpha\beta 0}. \tag{2}$$

Neglecting the zero-sequence terms, the dynamics of the VSC ac-side variables in an SRF ($\alpha\beta$ frame) is derived. Since the α and β components are orthogonal, all variables in an $\alpha\beta$ space can be treated as complex numbers, i.e., $x_{\alpha\beta} = x_\alpha + jx_\beta$. Adopting (2) and applying an $\alpha\beta$-to-dq-frame transformation $x_{dq} = x_{\alpha\beta}e^{-j\omega t}$, the dynamics of the VSC ac-side variables in an RRF (dq frame) is derived

$$v_{t,dq} = R_t i_{t,dq} + L_t \frac{di_{t,dq}}{dt} + j\omega L_t i_{t,dq} + v_{dq}. \tag{3}$$

Separating the real and imaginary terms, the dynamics of the d and q axes are deduced

$$R_t i_{t,d} + L_t \frac{di_{t,d}}{dt} = v_{t,d} + \omega L_t i_{t,q} - v_d \tag{4}$$

$$R_t i_{t,q} + L_t \frac{di_{t,q}}{dt} = v_{t,q} - \omega L_t i_{t,d} - v_q. \tag{5}$$

Based on (4) and (5), the structural diagram of the system in the rotating frame is obtained, as shown in Fig. 2, which contains the typical coupling terms.

Note that, in the conducted study of this paper, the dc-side dynamics are neglected, and it is assumed that the dc link voltage is fixed at a desired level by an ideal voltage source.

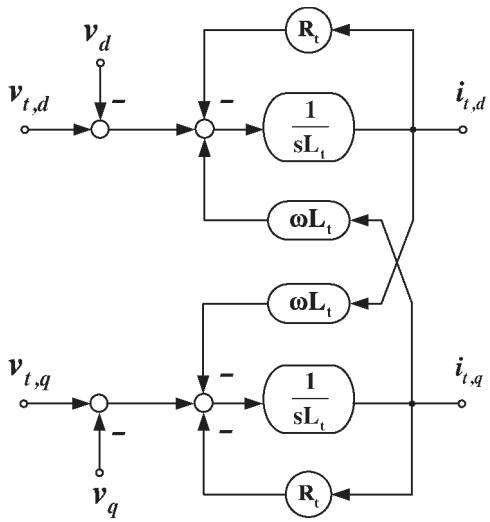

Fig. 2. Structural diagram of the test system in the RRF.

III. Conventional dq Current Controller

The conventional dq current control strategy is well known and widely studied in the literature [12], [15], [24]–[32]. In the following paragraphs, adopting the derived model in Section II-A, this approach is briefly reviewed.

Adopting (4) and (5), in order to achieve decoupled control of i_d and i_q, the inverter voltage should be controlled as follows [15]:

$$v_{t,d} = u_{c,d} - L_t \omega i_{t,q} + v_d \tag{6}$$

$$v_{t,q} = u_{c,q} + L_t \omega i_{t,d} + v_q \tag{7}$$

in which $u_{c,d}$ and $u_{c,q}$ are control signals of the d and q axes in the RRF, respectively. Substituting $v_{t,d}$ and $v_{t,q}$ from (6) and (7), respectively, in (3), the following decoupled system is deduced:

$$\begin{pmatrix} u_{c,d} \\ u_{c,q} \end{pmatrix} = L_t \begin{pmatrix} di_{t,d}/dt \\ di_{t,q}/dt \end{pmatrix} + \begin{pmatrix} R_t & 0 \\ 0 & R_t \end{pmatrix} \begin{pmatrix} i_{t,d} \\ i_{t,q} \end{pmatrix}. \tag{8}$$

Therefore, the transfer function of the decoupled system can be derived as

$$\mathbf{G_s}(\mathbf{s}) = \frac{K_s}{1 + sT_s} \tag{9}$$

in which the time constant $T_s = L_t/R_t$ and $K_s = 1/R_t$.

Note that, since $i_{t,d}$ and $i_{t,q}$ respond to $u_{c,d}$ and $u_{c,q}$ through a simple first-order transfer function, the control rules of (6) and (7) are completed by defining feedback loops and using simple first-order PI controllers [15]. Based on (6) and (7), the structural diagram of the current regulator based on PI controllers is depicted in Fig. 3 in which the voltage feedforwards and the coupling terms are shown.

The corresponding control loop is depicted in Fig. 4 in which the controller is represented by $\mathbf{G_R}(\mathbf{s})$. To model more precisely the behavior of the converter, the closed-loop system is accompanied by an equivalent transfer function $\mathbf{G_{pE}}$ representing the behavior of the pulsewidth modulation (PWM) generator of the converter, together with the additional time

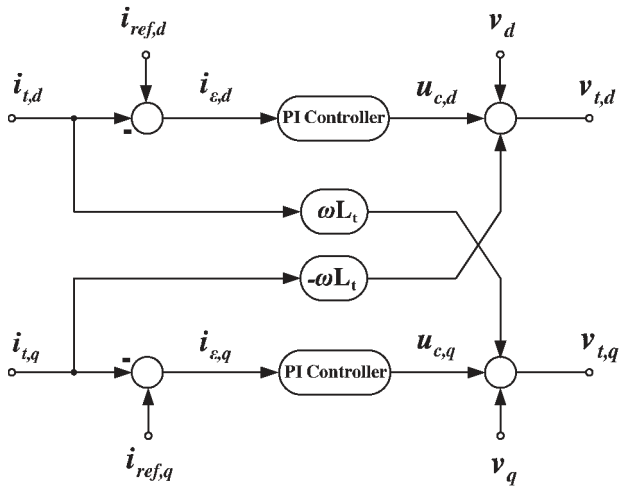

Fig. 3. Structural diagram of the conventional dq current controller.

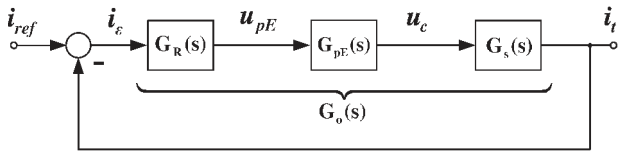

Fig. 4. Control loop for the current space phasor.

delay caused by the sampling and measurements, as defined in [1]. An equivalent sum of these delays is approximated by

$$\mathbf{G^s_{pE}}(\mathbf{s}) = \frac{K_{\rm cm}}{1 + sT_{\rm pE}} \tag{10}$$

which is a first-order element in an SRF. Note that the adopted transfer function corresponds to a pseudocontinuous representation of real phenomena considering the mean values of the electrical quantities. Therefore, the equivalent transfer function of $\mathbf{G^s_{pE}}$ in the RRF can be written as

$$\mathbf{G_{pE}}(\mathbf{s}) = \frac{K_{\rm cm}}{1 + (s + j\omega)T_{\rm pE}}. \tag{11}$$

The obtained transfer function shows a coupling term, i.e., $j\omega$, that must be evaluated in the magnitude of its effect. Since the switching frequency of the converter is considerably higher than the fundamental frequency and $T_{\rm pE}$ is considerably smaller than other time constants in the system, the coupling term $j\omega T_{\rm pE}$ can be neglected. Note that such a neglect results in ignoring the coupling between the two axes; however, due to its negligible magnitude, it does not have a major effect. Therefore

$$\mathbf{G_{pE}}(\mathbf{s}) = \frac{K_{\rm cm}}{1 + sT_{\rm pE}}. \tag{12}$$

Then, the controller is designed based on the open-loop transfer function $\mathbf{G_0}(\mathbf{s})$, as shown in Fig. 4, which is represented by

$$\mathbf{G_o}(\mathbf{s}) = \mathbf{G_R}(\mathbf{s})\mathbf{G_{pE}}(\mathbf{s})\mathbf{G_s}(\mathbf{s}). \tag{13}$$

Substituting $\mathbf{G_s}(\mathbf{s})$ and $\mathbf{G_{pE}}(\mathbf{s})$ from (9) and (12), respectively, in (13), the open-loop transfer function of the system is

derived as

$$\mathbf{G_o}(\mathbf{s}) = \mathbf{G_R}(\mathbf{s})\frac{K_{\rm cm}}{1+sT_{\rm pE}}\frac{K_s}{1+sT_s}. \tag{14}$$

A conventional PI controller is then adopted as $\mathbf{G_R}(\mathbf{s})$ in order to achieve the prespecified dynamics. Therefore

$$\mathbf{G_R}(\mathbf{s}) = \frac{1+sT_{\rm n}}{sT_{\rm i}}. \tag{15}$$

The controller time constant $T_{\rm n}$ is chosen to be equal to the dominant time constant T_s, which results in the simplification of (14), i.e.,

$$\mathbf{G_o}(\mathbf{s}) = \frac{K}{sT_{\rm i}(1+sT_{\rm pE})}. \tag{16}$$

Using the simplified transfer function in (16), the remaining parameter to design is the integration time constant $T_{\rm i}$ that can be determined by the usual criteria on the phase margin. Usually, $T_{\rm i}$ is chosen as $T_{\rm i} = 2KT_{\rm pE}$. This value corresponds to a classical case where the zero-crossing pulsation of the open-loop transfer function ω_0 is equal to $0.5(1/T_{\rm pE})$ [1].

It should be noted that, according to (8), adopting the feedforward signals theoretically results in a fully decoupled system. This perfect decoupling can be achieved only if the feedforward signals can precisely cancel the effect of the coupling terms, i.e., $\omega L_t i_d$ and $\omega L_t i_q$. However, in a real system, due to measurement errors, it is not practically possible to precisely determine the value of i_{dq}, L_t, and ω, and therefore, the ideal coupling term cancellation is impossible. Moreover, the system delays caused by the sampling and/or the PWM block also eventuate imperfect cancellation. Therefore, in a practical case, adopting the conventional control strategy cannot fully decouple the axes.

IV. Multivariable-PI *dq* Current Controller

In this section, based on the derived model in Section II-A, the multivariable-PI current controller is described, and its structural diagram is provided. Moreover, the applicability of the method to anisotropic three-phase systems is investigated, and it is shown that the method is capable of regulating currents in anisotropic systems such as synchronous motors with dissimilar impedances in the d and q axes [1].

Contrary to the conventional approach, which relies on the feedforward signals to eliminate the coupling, the multivariable-PI controller adopts plant inversion techniques to design a decoupled control system. Adopting the diagram in Fig. 2 or, equivalently, its dynamic representation in (3), the transfer function of the system is derived. Applying a Laplace transformation to (3), the following equation is derived:

$$V_t(s) = R_t I_t(s) + L_t s I_t(s) + j\omega L_t I_t(s) + V(s). \tag{17}$$

Since the grid voltage is fixed and imposed by the utility grid, one can add it to the output of the controller as a feedforward signal to cancel its effect. Therefore, subtracting $V(s)$ from both sides of (17), the transfer function of the system from $V_t - V$ to I_t is obtained as

$$\mathbf{G_s}(\mathbf{s}) = \frac{K_s}{1+(s+j\omega)T_s} \tag{18}$$

in which the time constant T_s is equal to L_t/R_t and $K_s = 1/R_t$, where the coupling between the d and q axes is represented by the term $j\omega T_s$. Substituting $\mathbf{G_s}$ and $\mathbf{G_{pE}}$ from (18) and (12), respectively, in (13), the open-loop transfer function of the system utilizing the multivariable-PI controller is deduced

$$\mathbf{G_o}(\mathbf{s}) = \mathbf{G_R}(\mathbf{s})\frac{K_{\rm cm}}{1+sT_{\rm pE}}\frac{K_s}{1+(s+j\omega)T_s}. \tag{19}$$

In order to achieve a normal polynomial without complex factors, $\mathbf{G_R}(\mathbf{s})$ is selected as a so-called multivariable-PI controller as follows:

$$\mathbf{G_R}(\mathbf{s}) = \frac{1+(s+j\omega)T_{\rm n}}{sT_{\rm i}}. \tag{20}$$

The controller time constant $T_{\rm n}$ is chosen to be equal to the dominant time constant of the system transfer function T_s allowing the simplification of (19), leading to

$$\mathbf{G_o}(\mathbf{s}) = \frac{K}{sT_{\rm i}(1+sT_{\rm pE})} \tag{21}$$

in which K is $K_{\rm cm}K_s$. The open-loop transfer function in (21) is now a normal polynomial form without complex factors, which means that the system is decoupled. The remaining parameter to design is the integration time constant $T_{\rm i}$, which can be determined by a usual criterion on the phase margin as follows:

$$T_{\rm i} = 2KT_{\rm pE}. \tag{22}$$

A. Structural Diagram of Multivariable-PI Controller

The multivariable-PI controller defined in (20) has a complex transfer function. Separating the real and imaginary parts, the controller can be written as

$$y_{R,d} + jy_{R,q} = \left(\frac{1+sT_{\rm n}}{sT_{\rm i}} + j\frac{\omega T_{\rm n}}{sT_{\rm i}}\right)(i_{\varepsilon,d} + ji_{\varepsilon,q}). \tag{23}$$

Therefore

$$y_{R,d} = \frac{1+sT_{\rm n}}{sT_{\rm i}}i_{\varepsilon,d} - \frac{\omega T_{\rm n}}{sT_{\rm i}}i_{\varepsilon,q} \tag{24}$$

$$y_{R,q} = \frac{1+sT_{\rm n}}{sT_{\rm i}}i_{\varepsilon,q} + \frac{\omega T_{\rm n}}{sT_{\rm i}}i_{\varepsilon,d}. \tag{25}$$

Equations (24) and (25) represent the control signals in both the d and q axes, which include the cross coupling terms. However, contrary to the conventional dq current controller in Section III, the coupling terms include integrators, which significantly reduce the effect of the axes on each other and results in practically decoupled axes. The structural diagram of the multivariable-PI controller is shown in Fig. 5. The feedforward

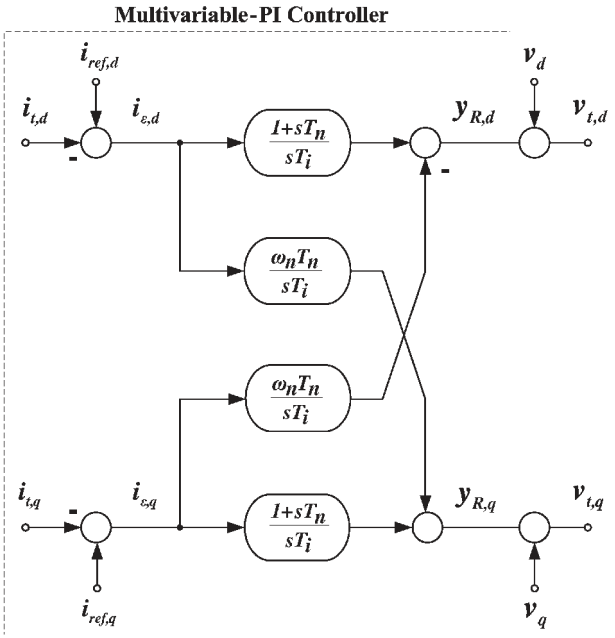

Fig. 5. Structural diagram of multivariable-PI controller with voltage feedforward.

signals adopted for rejecting the disturbances caused by the utility grid are also depicted in Fig. 5.

It should be noted that, since the multivariable-PI method does not rely on the feedforward signals, the system parameter uncertainties cannot significantly degrade its performance. A comparison between the multivariable-PI method and the conventional one in terms of immunity to the system parameter uncertainties is conducted and presented in Section V.

B. Multivariable-PI Controller for Anisotropic Systems

Applying the abc-to-dq transformation to anisotropic systems, the d- and q-axis parameters may differ. This is also the case for anisotropic synchronous motors in which the stator and rotor impedances, i.e., x_d and x_q, are different. If the information on the anisotropic system parameters is available, the multivariable-PI control strategy can be modified such that the effect of the imbalance is taken into account [1]. In the following paragraphs, adopting the test system in Fig. 6, which includes a synchronous motor and its driver, the structure of the multivariable-PI controller for anisotropic systems is detailed.

The dynamics of the test system in Fig. 6 can be expressed by [33], [34]

$$x_d\frac{di_d}{dt} = -\omega R i_d + n\omega x_q i_q + \omega u_d \tag{26}$$

$$x_q\frac{di_q}{dt} = -\omega R i_q - n\omega x_d i_d + \omega(u_q - u_p) \tag{27}$$

in which x_d and x_q represent the direct and quadrature impedances, which are assumed to be different. The stator currents and voltages are represented by i_{dq} and u_{dq}, respectively, in the RRF. Moreover, R stands for the stator resistance, n is the speed of the rotor, and u_p is the induced voltage given by $u_P = ni_e$ in which i_e is the excitation current. Note that, in the following paragraphs, contrary to Section III, a matrix analysis is adopted. The reason is that, due to different parameters of the d and q axes, it is not possible to utilize complex transfer functions. However, although the complex transfer function analysis is more straightforward, one can still use the matrix analysis for the isotropic case as well. It should be noted that the adopted bold letters represent the multiple-input–multiple-output transfer functions, and the italic-bold letters represent the system parameter matrices.

Adopting (26) and (27), the following matrix representation of the system is derived:

$$\begin{pmatrix} di_d/dt \\ di_q/dt \end{pmatrix} = \boldsymbol{A}\begin{pmatrix} i_d \\ i_q \end{pmatrix} + \boldsymbol{B}\begin{pmatrix} u_d \\ u_q - u_p \end{pmatrix} \tag{28}$$

in which

$$\boldsymbol{A} = \begin{pmatrix} -\omega R/x_d & n\omega x_q/x_d \\ -n\omega x_d/x_q & -\omega R/x_q \end{pmatrix} \tag{29}$$

$$\boldsymbol{B} = \begin{pmatrix} \omega/x_d & 0 \\ 0 & \omega/x_q \end{pmatrix}. \tag{30}$$

Applying the Laplace transform to (28), the following equation is deduced:

$$(s\boldsymbol{I} - \boldsymbol{A})\begin{pmatrix} i_d(s) \\ i_q(s) \end{pmatrix} = \boldsymbol{B}\begin{pmatrix} u_d(s) \\ u_q(s) - u_p(s) \end{pmatrix}. \tag{31}$$

Adopting (31), the system transfer function can be written as

$$\mathbf{G_s}(\mathbf{s}) = (s\boldsymbol{I} - \boldsymbol{A})^{-1}\boldsymbol{B}. \tag{32}$$

In order to eliminate the stationary error in the closed loop, the open-loop transfer function needs to have an integral behavior. Therefore

$$\mathbf{G_s}(\mathbf{s})\mathbf{G_R}(\mathbf{s}) = \frac{1/R}{sT_{\mathrm{i}}}\boldsymbol{I} \tag{33}$$

or equivalently

$$\mathbf{G_R}(\mathbf{s}) = \frac{1/R}{sT_{\mathrm{i}}}\mathbf{G_s}^{-1}(\mathbf{s}). \tag{34}$$

Substituting $\mathbf{G_s}(\mathbf{s})$ from (32) in (34), the following equation is resulted:

$$\mathbf{G_R}(\mathbf{s}) = \frac{1/R}{sT_{\mathrm{i}}}\boldsymbol{B}^{-1}(s\boldsymbol{I} - \boldsymbol{A}). \tag{35}$$

Adopting matrices $\boldsymbol{A}$ and $\boldsymbol{B}$ as defined in (29) and (30), respectively, $\mathbf{G_R}(\mathbf{s})$ is derived as the following matrix:

$$\mathbf{G_R}(\mathbf{s}) = \frac{1/R}{sT_{\mathrm{i}}}\begin{pmatrix} \frac{sx_d}{\omega} + R & -nx_q \\ nx_d & \frac{sx_q}{\omega} + R \end{pmatrix}. \tag{36}$$

Introducing the time constants $T_{sd} = x_d/\omega R$ and $T_{sq} = x_q/\omega R$, the multivariable-PI controller takes the

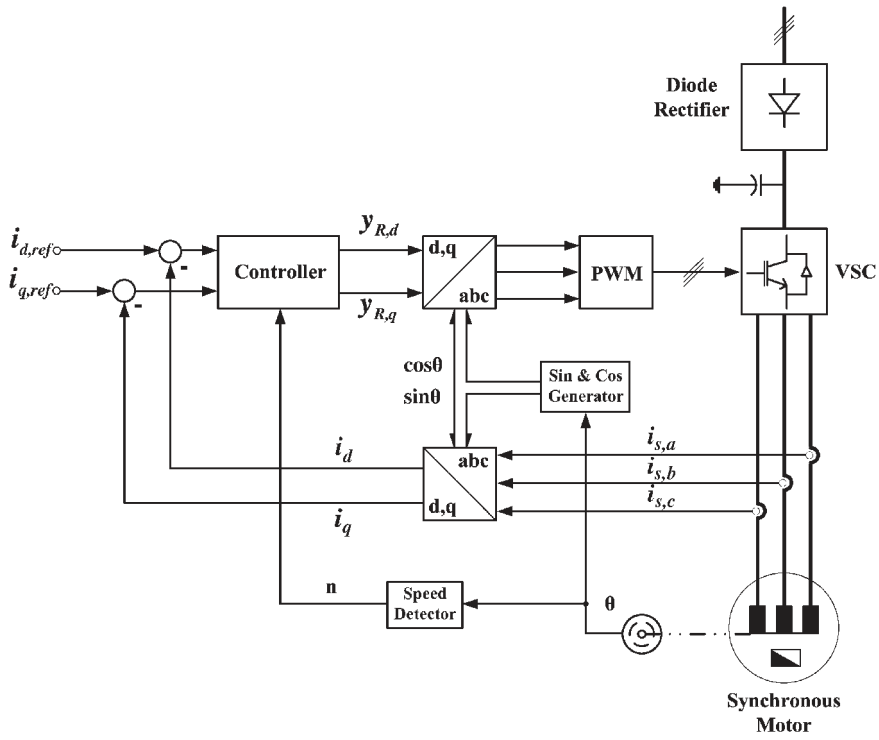

Fig. 6. Schematic diagram of a synchronous motor with different direct and quadrature impedances driven by a VSC.

following form:

$$\mathbf{G_R}(\mathbf{s}) = \begin{pmatrix} \frac{1+sT_{sd}}{sT_{\mathrm{i}}} & -n\frac{\omega T_{sq}}{sT_{\mathrm{i}}} \\ n\frac{\omega T_{sd}}{sT_{\mathrm{i}}} & \frac{1+sT_{sq}}{sT_{\mathrm{i}}} \end{pmatrix}. \tag{37}$$

Since there is no imaginary term in the elements of $\mathbf{G_R}(\mathbf{s})$, the direct and transversal components of the multivariable controller are the elements of the derived matrix in (37). In the direct branches, there are standard PI controllers with different time constants for each axis. Moreover, in the transversal branches, there are integral controllers, again with different time constants for each axis. Using this multivariable-PI controller, two decoupled systems for the direct and quadrature axes are achieved. The structural diagram of the controller is depicted in Fig. 7.

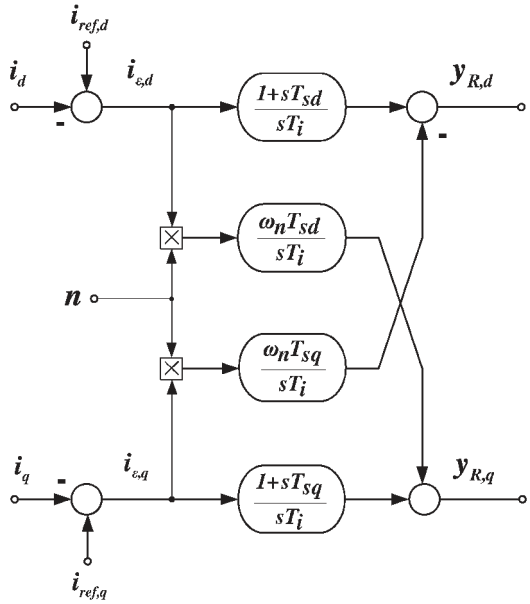

Fig. 7. Structural diagram of multivariable-PI controller for anisotropic systems.

V. Performance Evaluation

The purpose of this section is to experimentally evaluate the performance of the multivariable-PI controller and also to compare it with that of the conventional dq current control strategy. The presented test results show that the multivariable-PI controller has the following characteristics: 1) is capable of tracking the reference signals with a zero steady-state error; 2) has fast dynamics; 3) contrary to the conventional approach, provides practically decoupled d and q current axes; and 4) is much less susceptible to the system parameter uncertainties compared to the conventional controller. Note that, in the following tests, the multivariable-PI and conventional controllers are designed based on similar design criteria, e.g., phase and gain margins.

To evaluate the performance of the controllers, two sets of tests are conducted for each control strategy: 1) step-down and step-up in the d-axis reference value while that of the q-axis is kept constant and 2) step-down and step-up in the q-axis reference value while that of the d-axis is kept constant. Moreover, to evaluate the sensitivity of the conventional and multivariable-PI controllers to the system parameter uncertainties, a test similar to the aforementioned reference-tracking case studies is conducted for each controller while the parameters of the system, i.e., R_t and L_t, are deliberately mismeasured.

Adopting the test system in Fig. 1 and the corresponding parameters in Table I, the three-phase experimental setup is

Fig. 8. Experimental setup.

implemented. Fig. 8 shows a photograph of the setup. To implement the control strategies and signal processing algorithms, a field-programmable gate array (FPGA)-based controller, which provides a C programming environment, is used. The adopted FPGA is an XC4010PC84 FPGA manufactured by XILINX. The control and signal processing algorithms are first discretized using the bilinear method [35] and then developed into C codes. It should be noted that, in order to achieve perfect isolation between the power and control circuits, optic-based gate drivers are adopted for driving insulated-gate bipolar transistors (IGBTs).

A. Reference-Tracking Test in d-Axis

In this section, the performance of both current regulation schemes is experimentally evaluated subsequent to two step changes in the reference value of the d-axis. It is shown that, using the conventional control strategy, subsequent to the step changes in the d-axis, a nonnegligible transient is experienced in the q one, which verifies that the axes are not fully decoupled. However, conducting a similar test for the multivariable-PI controller, it is verified that, using the multivariable controller, the axes are much less coupled.

1) Conventional Controller: The inverter in Fig. 1 initially injects 0.4 p.u. of the q-component and -0.1 p.u. of the d-component of the currents. At the time instant of 0.071 s, the d-component steps up to -0.9 p.u., and at $t = 0.101$ s, it steps down to -0.1 p.u. while the reference value for the q-component is kept constant during the whole process. Fig. 9(a) depicts the point of common coupling (PCC) voltages, which remain unchanged during and subsequent to the step changes. However, upon each step change, the line currents and their corresponding d-component change to track the reference value changes in almost 1 ms with a zero steady-state error, as shown in Fig. 9(b) and (c). Although the reference value of the q-axis is constant, however, subsequent to each change in the d-axis, the q-axis also experiences transients, which are not negligible and last for almost 15 ms, as shown in Fig. 9(d). The latter transients verify that the conventional current control strategy suffers from coupled axes.

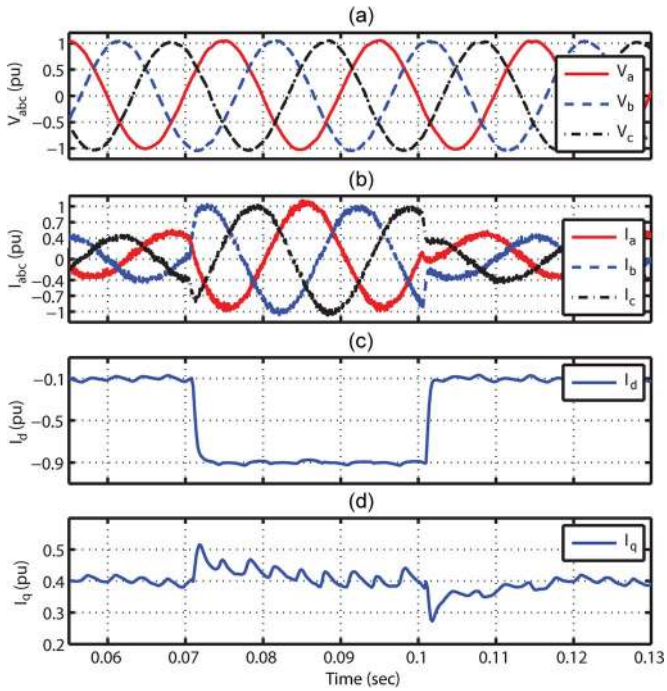

Fig. 9. Experimental results of the transient response of the conventional controller during step changes in d-axis. (a) PCC voltages. (b) Line currents. (c) d-component of the currents. (d) q-components of the currents.

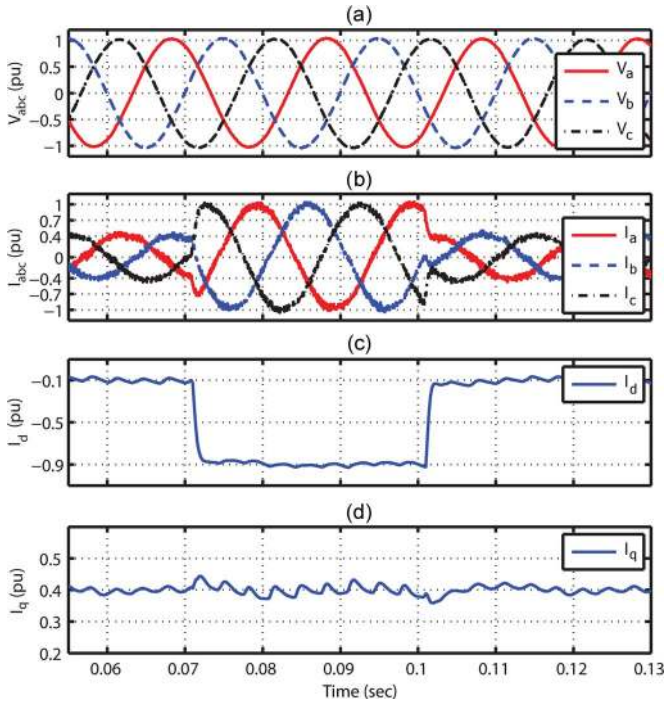

Fig. 10. Experimental results of the transient response of multivariable-PI controller during step changes in d-axis. (a) PCC voltages. (b) Line currents. (c) d-component of the currents. (d) q-components of the currents.

2) Multivariable-PI Controller: The VSC adopted in the test system in Fig. 1 initially injects 0.4 p.u. of the q-component and -0.1 p.u. of the d-component of the currents. Keeping the q-axis reference value constant, at the time instant of 0.071 s, the reference value of the d-component steps up to -0.9 p.u. Moreover, at $t = 0.101$ s, the d-axis reference value is set back to -0.1 p.u. Fig. 10(a) shows the PCC voltages, which are

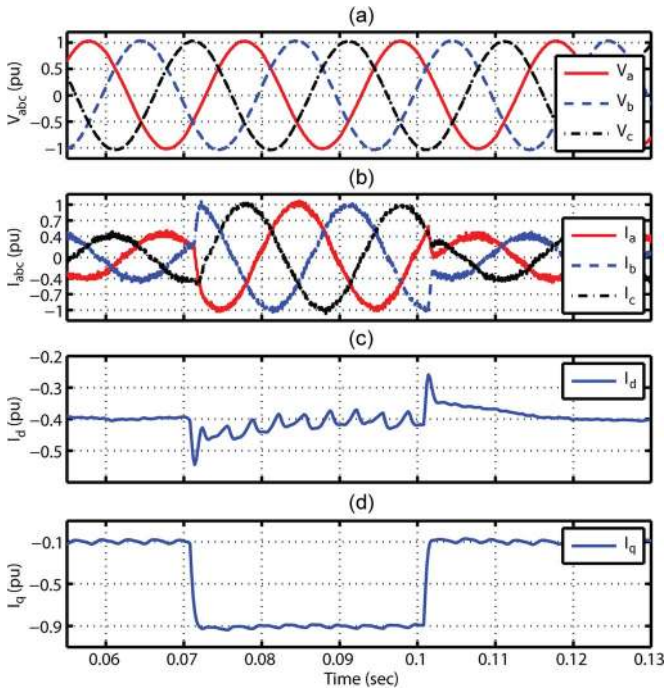

Fig. 11. Experimental results of the transient response of the conventional controller during step changes in q-axis. (a) PCC voltages. (b) Line currents. (c) d-component of the currents. (d) q-components of the currents.

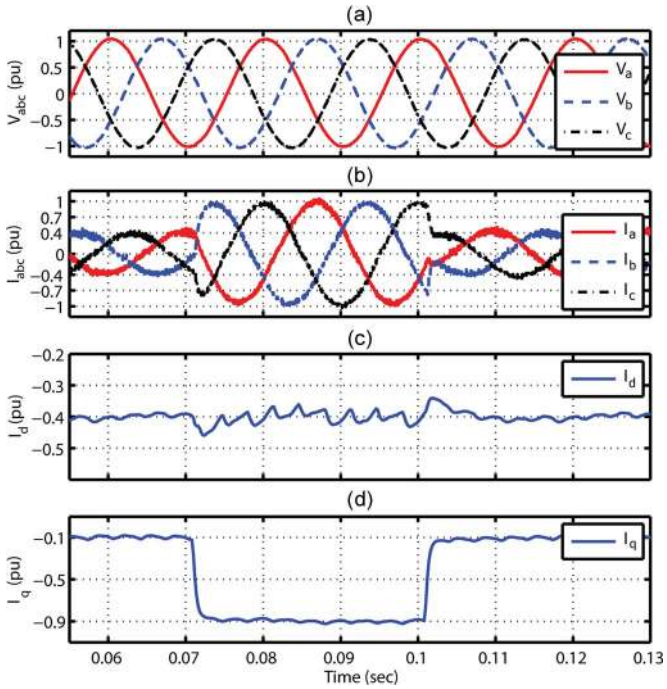

Fig. 12. Experimental results of the transient response of multivariable-PI controller during step changes in q-axis. (a) PCC voltages. (b) Line currents. (c) d-component of the currents. (d) q-components of the currents.

regulated at the rated value by the grid and do not change. Subsequent to each change in the d-axis reference value, the controller regulates the currents at the desired level, as shown in Fig. 10(b). Fig. 10(c) depicts that, subsequent to each step change in the d-axis, the d-component of the currents is regulated at the desired level in almost 1 ms with a zero steady-state error. However, contrary to the conventional controller, subsequent to each step change in the d-axis, the q-component of the currents experiences very short and negligible transients.

Comparing Figs. 9 and 10 verifies that the performance of the multivariable-PI controller in terms of tracking the step changes in the d-axis is comparable and similar to that of the conventional controller. However, contrary to the conventional controller, upon the step changes in the d-axis, the multivariable-PI controller imposes much less transients on the q-axis.

B. Reference-Tracking Test in q-Axis

In this section, in order to verify the superior performance of the multivariable-PI controller in terms of decoupling the axes during the step changes in the q-axis, a similar test to that of the previous section is carried out. However, the step changes are imposed on the q-axis, and the capability of the controllers in terms of decoupling the axes is evaluated and compared.

1) Conventional Controller: The inverter in Fig. 1 initially injects -0.4 p.u. of the d-component and -0.1 p.u. of the q-component of the current. At the time instant of 0.071 s, the q-component steps up to -0.9 p.u., and at $t = 0.101$ s, it steps down to -0.1 p.u. while the reference value for the d-component is kept constant during the whole process. Fig. 11(a) depicts the PCC voltages, which are dictated by the grid and regulated at the rated value during the test. However, upon each step change, the q-component of the currents and, consequently, the abc currents change to track the reference value changes in almost 1 ms with the zero steady-state error, as shown in Fig. 11(b) and (c). Although the reference value of the d-axis is constant, however, subsequent to each change in the q-axis, the d-axis current undergoes transients, which are not negligible and last for almost 15 ms, as shown in Fig. 11(d), which verifies that the conventional current control strategy suffers from coupled axes.

2) Multivariable-PI Controller: The VSC adopted in the test system in Fig. 1 initially injects -0.4 p.u. of the d-component and -0.1 p.u. of the q-component of the currents. Keeping the d-axis reference value constant, at the time instant of 0.071 s, the reference value of the q-component steps up to -0.9 p.u. Moreover, at $t = 0.101$ s, the q-axis reference value is set back to -0.1 p.u. Fig. 12(a) shows the PCC voltages, which are kept constant at the rated value by the grid and do not change. Subsequent to each change in the q-axis reference value, the controller regulates the currents at the desired level, as shown in Fig. 12(b). Fig. 12(c) depicts that, subsequent to each step change in the q-axis, the q-component of the currents is regulated at the desired level in almost 1 ms with a zero steady-state error. However, contrary to the conventional controller, subsequent to each step change in the q-axis, the d-component of the currents experiences very short and negligible transients, as shown in Fig. 12(d).

Comparing Figs. 11 and 12, the performance of the multivariable-PI controller in terms of tracking the step changes in the q-axis is comparable to that of the conventional controller. However, contrary to the conventional controller, upon the step changes in the q-axis, the multivariable-PI controller provides superior axis decoupling capability compared to the conventional approach.

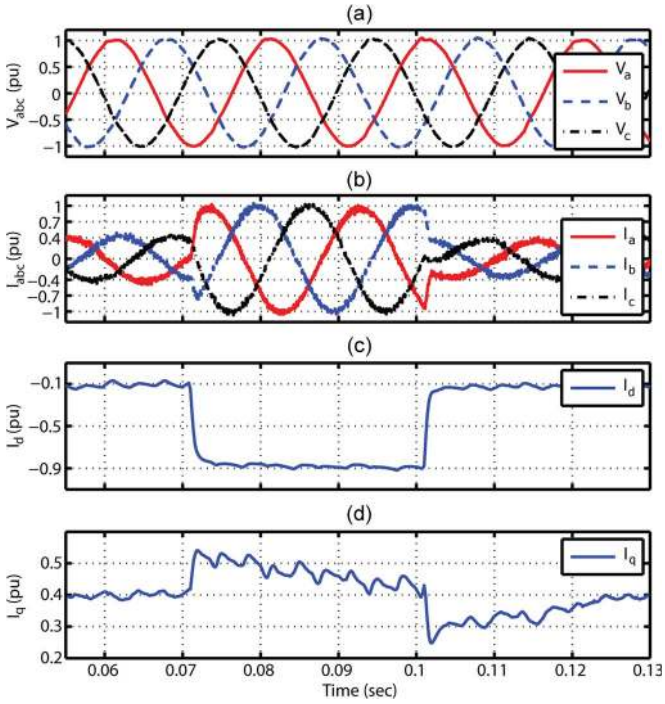

Fig. 13. Experimental results of the transient response of the conventional controller during step changes in d-axis while the parameters are mismeasured. (a) PCC voltages. (b) Line currents. (c) d-component of the currents. (d) q-components of the currents.

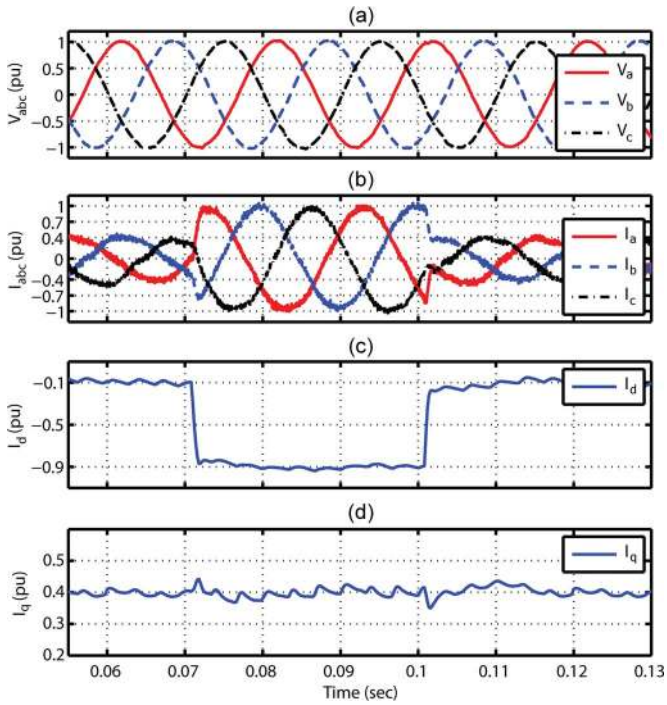

Fig. 14. Experimental results of the transient response of multivariable-PI controller during step changes in d-axis while the parameters are mismeasured. (a) PCC voltages. (b) Line currents. (c) d-component of the currents. (d) q-components of the currents.

C. Sensitivity to System Parameter Uncertainties

In this section, the sensitivities of the conventional and multivariable-PI controllers to the system parameters, i.e., R_t and L_t, are evaluated. For each controller, a test similar to what is conducted in Section V-A is carried out. According to Table I, the real values of R_t and L_t are 0.15 Ω and 5 mH, respectively. However, to design the controllers, it is assumed that, due to measurement errors, the estimated values of R_t and L_t are 0.3 Ω and 2.5 mH, respectively.

1) Conventional Controller: The inverter in Fig. 1 initially injects 0.4 p.u. of the q-component and -0.1 p.u. of the d-component of the currents. At the time instant of 0.071 s, the d-component steps up to -0.9 p.u., and at $t = 0.101$ s, it steps down to -0.1 p.u. while the reference value for the q-component is kept constant during the whole process. Fig. 13(a) depicts the PCC voltages, which are dictated by the grid and regulated at the rated value during the test. However, upon each step change, the d-component of the currents and, consequently, the abc currents change to track the reference value changes in almost 1 ms with a zero steady-state error, as shown in Fig. 13(b) and (c). Although the reference value of the q-axis is constant, however, subsequent to each change in the q-axis, the d-axis undergoes relatively long transients, which are not negligible and last more than one cycle, as shown in Fig. 13(d), which verifies that the conventional current control strategy is sensitive to the system parameter uncertainties. As mentioned in Section III, the reason is that the conventional controller relies on the feedforward signals to achieve a decoupled system, and therefore, nonideal feedforward signals result in the imperfect cancellation of coupling terms and lead to more severe axis coupling.

2) Multivariable-PI Controller: The VSC adopted in the test system in Fig. 1 initially injects 0.4 p.u. of the q-component and -0.1 p.u. of the d-component of the currents. Keeping the q-axis reference value constant, at the time instant of 0.071 s, the reference value of the d-component steps up to -0.9 p.u. Moreover, at $t = 0.101$ s, the d-axis reference value is set back to -0.1 p.u. Fig. 14(a) shows the PCC voltages, which are dictated by the grid. Subsequent to each change in the d-axis reference value, the controller regulates the currents at the desired level, as shown in Fig. 14(b). Fig. 14(c) depicts that, subsequent to each step change in the d-axis, the d-component of the currents is regulated at the desired level in almost 1 ms with a zero steady-state error. However, contrary to the conventional controller, subsequent to each step change in the q-axis, the q-component of the currents experiences very short and negligible transients, as shown in Fig. 14(d).

Comparing Figs. 13 and 14 verifies that the multivariable-PI controller is much less sensitive to the system parameter uncertainties compared to the conventional approach. The reason is that the conventional controller relies on the feedforward signals and system parameter measurements while the multivariable-PI approach benefits from plant inversion to regulate the currents.

VI. Conclusion

A multivariable-PI-based vector control strategy for the current regulation of VSCs has been presented. Similar to the conventional current control strategies, the multivariable-PI method can independently regulate the direct and quadrature components of the current at desired reference levels while it does not impose excessive structural complexity compared to

the conventional approaches and can be easily implemented in digital environments. The performance of the multivariable-PI method is experimentally evaluated and it is shown that the method has the following characteristics:

1) can track the d and q current reference signals with zero steady-state errors;
2) is as fast as the conventional approach;
3) has superior axis decoupling capability compared to the conventional approach;
4) is much less sensitive to the system parameter uncertainties compared to the conventional approach.

Moreover, it has been shown that, contrary to the conventional approach, which is only tailored for balanced systems, the multivariable-PI controller can be manipulated to be adopted in anisotropic systems, e.g., in anisotropic synchronous motors driven by VSCs.

ACKNOWLEDGMENT

The authors would like to thank Prof. H. Bühler, the former head of the Industrial Electronics Laboratory, Ecole Polytechnique Fédérale de Lausanne, for his valuable contribution to this paper as the main idea of the conducted studies was initiated by him. The authors would also like to dedicate this paper to him.

REFERENCES

[1] H. Bühler, *Réglage des Systèmes d'Électronique de Puissance*, vol. 1, 2 and 3, *Théorie*. Lausanne, Switzerland: PPUR, Presses Polytechniques et Universitaires Romandes, 1997.

[2] S. B. Kjaer, J. K. Pedersen, and F. Blaabjerg, "A review of single-phase grid-connected inverters for photovoltaic modules," *IEEE Trans. Ind. Appl.*, vol. 41, no. 5, pp. 1292–1306, Sep./Oct. 2005.

[3] E. Villanueva, P. Correa, J. Rodríguez, and M. Pacas, "Control of a single-phase cascaded H-bridge multilevel inverter for grid-connected photovoltaic systems," *IEEE Trans. Ind. Electron.*, vol. 56, no. 11, pp. 4399–4406, Nov. 2009.

[4] B. C. Rabelo, W. Hofmann, J. Lucas da Silva, R. Gaiba de Oliveira, and S. R. Silva, "Reactive power control design in doubly fed induction generators for wind turbines," *IEEE Trans. Ind. Electron.*, vol. 56, no. 10, pp. 4154–4162, Oct. 2009.

[5] M. Saeedifard, R. Iravani, and J. Pou, "A space vector modulation strategy for a back-to-back five-level HVDC converter system," *IEEE Trans. Ind. Electron.*, vol. 56, no. 2, pp. 452–466, Feb. 2009.

[6] H. Akagi, "Active harmonic filters," *Proc. IEEE*, vol. 93, no. 12, pp. 2128–2141, Dec. 2005.

[7] V. F. Corasaniti, M. B. Barbieri, P. L. Arnera, and M. I. Valla, "Hybrid active filter for reactive and harmonics compensation in a distribution network," *IEEE Trans. Ind. Electron.*, vol. 56, no. 3, pp. 670–677, Mar. 2009.

[8] J. Miret, M. Castilla, J. Matas, J. M. Guerrero, and J. C. Vasquez, "Selective harmonic-compensation control for single-phase active power filter with high harmonic rejection," *IEEE Trans. Ind. Electron.*, vol. 56, no. 8, pp. 3117–3127, Aug. 2009.

[9] P. G. Barbosa, L. G. B. Rolim, and E. H. Watanabe, "Control strategy for grid-connected dc ac with load power factor correction converters," *Proc. Inst. Elect. Eng.—Gener., Transm. Distrib.*, vol. 145, no. 5, pp. 487–491, Sep. 1998.

[10] L. Hassaine, E. Olias, J. Quintero, and M. Haddadi, "Digital power factor control and reactive power regulation for grid-connected photovoltaic inverter," *Renew. Energy*, vol. 34, no. 1, pp. 315–321, Jan. 2009.

[11] F. Blaabjerg, R. Teodorescu, M. Liserre, and A. V. Timbus, "Overview of control and grid synchronization for distributed power generation systems," *IEEE Trans. Ind. Electron.*, vol. 53, no. 5, pp. 1398–1409, Oct. 2006.

[12] M. P. Kazmierkowski and L. Malesani, "Current control techniques for three-phase voltage-source PWM converters: A survey," *IEEE Trans. Ind. Electron.*, vol. 45, no. 5, pp. 691–703, Oct. 1998.

[13] E. Song, A. F. Lynch, and V. Dinavahi, "Experimental validation of nonlinear control for a voltage source converter," *IEEE Trans. Control Syst. Technol.*, vol. 17, no. 5, pp. 1135–1144, Sep. 2009.

[14] A. Gensior, H. Sira-Ramírez, J. Rudolph, and H. Güldner, "On some nonlinear current controllers for three-phase boost rectifiers," *IEEE Trans. Ind. Electron.*, vol. 56, no. 2, pp. 360–370, Feb. 2009.

[15] C. Schauder and H. Mehta, "Vector analysis and control of advanced static VAR compensators," *Proc. Inst. Elect. Eng.—C*, vol. 140, no. 4, pp. 299–306, Jul. 1993.

[16] D. N. Zmood and D. G. Holmes, "Stationary frame current regulation of PWM inverters with zero steady-state error," *IEEE Trans. Power Electron.*, vol. 18, no. 3, pp. 814–822, May 2003.

[17] R. Teodorescu, F. Blaabjerg, M. Liserre, and P. C. Loh, "Proportional-resonant controllers and filters for grid-connected voltage-source converters," *Proc. Inst. Elect. Eng.—Electr. Power Appl.*, vol. 153, no. 5, pp. 750–762, Sep. 2006.

[18] G. Shen, X. Zhu, J. Zhang, and D. Xu, "A new feedback method for PR current control of LCL-filter based grid-connected inverter," *IEEE Trans. Ind. Electron.*, vol. 57, no. 6, pp. 2033–2041, Jun. 2010. 10.1109/TIE.2010.2040552.

[19] H. Abu-Rub, J. Guzinski, Z. Krzeminski, and H. A. Toliyat, "Predictive current control of voltage-source inverters," *IEEE Trans. Ind. Electron.*, vol. 51, no. 3, pp. 585–593, Jun. 2004.

[20] P. Zanchetta, D. B. Gerry, V. G. Monopoli, J. C. Clare, and P. W. Wheeler, "Predictive current control for multilevel active rectifiers with reduced switching frequency," *IEEE Trans. Ind. Electron.*, vol. 55, no. 1, pp. 163–172, Jan. 2008.

[21] J. C. Moreno, J. M. Espí Huerta, R. G. Gil, and S. A. González, "A robust predictive current control for three-phase grid-connected inverters," *IEEE Trans. Ind. Electron.*, vol. 56, no. 6, pp. 1993–2004, Jun. 2009.

[22] Y. A. I. Mohamed and E. F. El-Saadany, "An improved deadbeat current control scheme with a novel adaptive self-tuning load model for a three-phase PWM voltage-source inverter," *IEEE Trans. Ind. Electron.*, vol. 54, no. 2, pp. 747–759, Apr. 2007.

[23] O. Kukrer, H. Komurcugil, and A. Doganalp, "A three-level hysteresis function approach to the sliding-mode control of single-phase UPS inverters," *IEEE Trans. Ind. Electron.*, vol. 56, no. 9, pp. 3477–3486, Sep. 2009.

[24] M. Liserre, R. Teodorescu, and F. Blaabjerg, "Multiple harmonics control for three-phase grid converter systems with the use of PI-RES current controller in a rotating frame," *IEEE Trans. Power Electron.*, vol. 21, no. 3, pp. 836–841, May 2006.

[25] A. Yazdani and R. Iravani, "A unified dynamic model and control for the voltage-sourced converter under unbalanced grid conditions," *IEEE Trans. Power Del.*, vol. 21, no. 3, pp. 1620–1629, Jul. 2006.

[26] H. Song and K. Nam, "Dual current control scheme for PWM converter under unbalanced input voltage conditions," *IEEE Trans. Ind. Electron.*, vol. 46, no. 5, pp. 953–959, Oct. 1999.

[27] S. Zhang, K.-J. Tseng, D. M. Vilathgamuwa, T. D. Nguyen, and X.-Y. Wang, "Design of a robust grid interface system for PMSG-based wind turbine generators," *IEEE Trans. Ind. Electron.*, vol. 58, no. 1, pp. 316–328, Jan. 2011.

[28] E. Twining and D. G. Holmes, "Grid current regulation of a three-phase voltage source inverter with an LCL input filter," *IEEE Trans. Power Electron.*, vol. 18, no. 3, pp. 888–895, May 2003.

[29] B. Saritha and P. A. Jankiraman, "Observer based current control of single-phase inverter in DQ rotating frame," in *Proc. Int. Conf. Power Electron., Drives, Energy Syst.*, Dec. 2006, pp. 1–5.

[30] A. Rufer, B. Bahrani, S. Kenzelmann, and L. Lopes, "Vector control of single-phase voltage source converters based on fictive axis emulation," in *Proc. 1st IEEE ECCE*, Sep. 2009, pp. 2689–2695.

[31] H. Komurcugil, "Steady-state analysis and passivity-based control of single-phase PWM current-source inverters," *IEEE Trans. Ind. Electron.*, vol. 57, no. 3, pp. 1026–1030, Mar. 2010.

[32] M. Castilla, J. Miret, J. Matas, L. García de Vicuña, and J. M. Guerrero, "Control design guidelines for single-phase grid-connected photovoltaic inverters with damped resonant harmonic compensators," *IEEE Trans. Ind. Electron.*, vol. 56, no. 11, pp. 4492–4501, Nov. 2009.

[33] G. Foo and M. F. Rahman, "Sensorless direct torque and flux-controlled IPM synchronous motor drive at very low speed without signal injection," *IEEE Trans. Ind. Electron.*, vol. 57, no. 1, pp. 395–403, Jan. 2010.

[34] M. Nemec, K. Drobnič, D. Nedeljković, and V. Ambrožič, "Direct current control of a synchronous machine in field coordinates," *IEEE Trans. Ind. Electron.*, vol. 56, no. 10, pp. 4052–4061, Oct. 2009.

[35] A. V. Oppenheim and R. W. Schafer, *Discrete-Time Signal Processing*. Englewood Cliffs, NJ: Prentice-Hall, 1999.

Behrooz Bahrani (S'07) received the B.Sc. degree in electrical engineering from the Sharif University of Technology, Tehran, Iran, in 2006, and the M.Sc. degree in electrical engineering from the University of Toronto, Toronto, ON, Canada, in 2008. He is currently working toward the Ph.D. degree at Ecole Polytechnique Fédérale de Lausanne, Lausanne, Switzerland.

From May to November 2008, he was a Research Intern with the ABB Corporate Research, Dättwil-Baden, Switzerland. His research interests include power electronics and its applications in power and traction systems.

Stephan Kenzelmann (S'09) was born in Zeneggen, Switzerland, in 1982. He received the M.Sc. degree in electrical engineering from the Ecole Polytechnique Fédérale de Lausanne, Lausanne, Switzerland, in 2007, where he is currently working toward the Ph.D. degree in the Industrial Electronics Laboratory.

His research interests include single-phase control methods, multilevel converter control, and research and development of new power electronic systems for dc power transmission.

Alfred Rufer (M'95–SM'01–F'06) received the M.S. degree from the Ecole Polytechnique Fédérale de Lausanne (EPFL), Lausanne, Switzerland, in 1976.

In 1978, he was with ABB, Turgi, Switzerland, where he was involved in the fields of power electronics and control, such as high-power variable frequency converters for drives, and where he was a Group Leader involved with power electronic development in 1985. In 1993, he was an Assistant Professor with the EPFL, where, since 1996, he has been a Full Professor and the Head of the Industrial Electronics Laboratory (LEI). The LEI is active in power electronics used in energy conversion and energy storage and in the modeling and simulation of systems, including control strategies and control circuits. He has authored or coauthored many publications on power electronics and applications, such as for multilevel converters or for different energy-storage systems. He is the holder of several patents.